Insights into the aftereffects phenomenon in solids based on DFT and time-differential perturbed γ-γ angular correlation studies in ^{111}In ($\rightarrow$ ^{111}Cd)-doped tin oxides

G. N. Darriba,[1,*] E. L. Muñoz,[2] D. Richard,[3] A. P. Ayala,[4] A. W. Carbonari,[5] H. M. Petrilli,[6] and M. Rentería[1,†]

[1]*Departamento de Física and Instituto de Física La Plata [IFLP, Consejo Nacional de Investigaciones Científicas y Técnicas (CONICET) La Plata], Facultad de Ciencias Exactas, Universidad Nacional de La Plata, CC 67, 1900 La Plata, Argentina*

[2]*Facultad de Ingeniería, Universidad Nacional de La Plata, 1900 La Plata, Argentina*

[3]*Centro de Tecnología de Recursos Minerales y Cerámica (CETMIC, CONICET La Plata-CIC PBA-UNLP), Camino Centenario y 506, CC 49, (B1897ZCA), M. B. Gonnet, Buenos Aires, Argentina*

[4]*Departamento de Física, Universidade Federal do Ceará, Fortaleza, CE, 60644-900, Brazil*

[5]*Instituto de Pesquisas Energéticas y Nucleares (IPEN) CNEN/SP, 05508-000 São Paulo, Brazil*

[6]*Instituto de Física, Universidade de São Paulo, Caixa Postal 66318, 05315-970 São Paulo, Brazil*

(Received 31 December 2021; accepted 15 March 2022; published 2 May 2022)

Recently, a model based on a combined *ab initio*/time-differential perturbed γ-γ angular correlation (TDPAC) study in the ^{111}In($\rightarrow$ ^{111}Cd)-doped SnO_2 semiconductor was proposed to enlighten the origin of the dynamic hyperfine interactions (HFIs) observed in oxides after the electron-capture (EC) decay of the probe nucleus of the ^{111}In parent. It was demonstrated that both the EC as well as the acceptor level introduced by the Cd impurity can contribute to the variation of the electric-field gradient (EFG) at the Cd site (responsible for this phenomenon) due to charge fluctuations of the electronic holes created [Darriba *et al.*, J. Phys. Chem. C **122**, 17423 (2018)]. To disentangle both effects, we performed here TDPAC reversible experiments in ^{111}In($\rightarrow$ ^{111}Cd)-doped SnO in the temperature range 20–900 K and a complete electronic structure density functional theory study of the Cd-doped SnO system as a function of the charge state (q) of the impurity. The isovalent ^{111}Cd probe impurity in this isocationic oxide was selected to demonstrate that the acceptor character of the probe is not a necessary condition to observe this electronic phenomenon when the EC is already present. A majority fraction of probes sensed a time-dependent HFI (HFI1) for all temperatures, and the unexpected minority always sensed a static interaction (HFI2). Comparing results from these experiments, the *ab initio* calculations of the EFG tensor and defect formation energies, HFI1 and HFI2, were assigned to ^{111}Cd probes localized at substitutional Sn sites free of defects [with the valence band (VB) completely filled, $q = 0$] and with an electronic hole trapped ($q = 1+$), respectively. In addition, we show that the systems with charge state between these values have very similar formation energies at the top of the VB and different predicted EFGs, giving support from first principles to the existence of random fluctuations between different EFGs, necessary in the construction of the on-off perturbation factor used. We demonstrate that all the probes fill their electronic holes before the TDPAC time window except the outermost one, giving a quantification of the number of electronic holes involved in the production of the dynamic effect, only one in SnO. The probes related to HFI2 reach their stable electronic configuration ($q = 1+$) before the emission of the first γ ray (γ_1) of the γ-γ cascade, while those related to HFI1 fill the last hole after the emission of γ_1, producing the dynamic interaction. Enlighted by these results and reviewing TDPAC experiments from the literature using probes with different nuclear decay characteristics, we concluded that, in the absence of EC decay of the probe nucleus of the parent, any probe impurity introducing acceptor or donor states (in semiconductors and insulators) whose ionization changes the EFG should observe a time-dependent HFI provided the lifetime of the nuclear levels that feed the γ_1 level and this level itself is shorter than the lifetime of the recovery process (i.e., the lifetime of the electronic holes or the ionized donor electrons).

DOI: 10.1103/PhysRevB.105.195201

I. INTRODUCTION

In condensed matter physics, the inclusion of impurities in the host lattice of oxide semiconductors plays a fundamental role, generating compounds that can develop unexpected physical properties [1–4]. A possible way to understand the modifications introduced by the doping impurity is to observe at a subnanoscale level what happens at the site where the impurity is located. Experimentally, this can be performed with nuclear solid-state techniques that rely on the use of the impurity itself as a probe atom. By these means, the impurity works as an instrument that measures key properties at the site where it is localized. In this sense, the time-differential perturbed γ-γ angular correlations (TDPAC) technique has been extensively applied to the study of doped semiconductors and insulators [5,6]. This technique is based on the

*darriba@fisica.unlp.edu.ar
†renteria@fisica.unlp.edu.ar

measurement of hyperfine interactions (HFIs) between the nuclear electric quadrupole moment (or magnetic dipole moment) of the probe nucleus and the extranuclear electric-field gradient (EFG) tensor (or magnetic hyperfine field) at the probe site [7]. The high sensitivity of the EFG to the nonspherical symmetry of the electronic density very close to the nucleus of the probe and the high precision of the TDPAC spectroscopy in its determination convert this technique into a powerful tool for the study of subtle changes in the electronic structure in the close surrounding of the probe atom, which is generally an impurity (but may also be a native atom) in the host semiconductor. This experimental method is useful to determine the temperature dependence of the EFG because its sensitivity is temperature independent, a great advantage that other hyperfine techniques do not present. In many binary oxides studied with the (^{111}In $\rightarrow$) ^{111}Cd TDPAC probe, challenging time-dependent HFIs were sometimes observed and attributed to the so-called *aftereffects* (AE) phenomenon after the electron-capture (EC) decay of the parent of the ^{111}In probe (ECAE) [7–17]. It is well known that the EC creates many electronic holes at the ^{111}Cd atom through Auger processes, almost all of them diffusing fast enough (in less than picoseconds) in such a way that this dynamic effect is not seen by the time window of the TDPAC measurement. Nevertheless, the latest electronic holes to be ionized could produce a dynamic HFI [7,8,18]. This interesting effect is characterized by a strong dampening of the spectra in approximately the first 10–50 ns (after this range, the already reduced anisotropy remains constant in the spectra), dampening which usually increases as the measuring temperature decreases to room temperature (RT). This behavior is reversible with measuring temperature, and the anisotropy (i.e., the amplitude of the spectrum) is fully recovered at high temperature. This effect, instead of being a real problem investigating the local structure of the host, is revealed to be an excellent laboratory to study the charge states produced by the doping probe.

Recently, we reported a complete study of structural, electronic, and hyperfine properties in ^{111}In($\rightarrow$ ^{111}Cd)-doped rutile SnO_2 [7] showing that, to ensure a correct interpretation of the time-dependent (*dynamic*) HFIs observed, a combined experimental and *ab initio* approach is essential. Previously, this approach had been successfully applied to the study of static HFIs in oxide semiconductors doped with ^{111}Cd [19–23] and ^{181}Ta as probe atoms [24–28]. In ^{111}In-doped SnO_2, the two time-dependent HFIs observed at substitutional ^{111}Cd sites were analyzed with an on-off perturbation factor, proposed by Bäverstam *et al.* [18]. In the model proposed in Ref. [7], each ^{111}Cd probe nucleus senses a dynamic HFI, due to time-dependent EFGs coming from fluctuations among different charge states of the ^{111}Cd atom, until the atom arrives to a final static electronic configuration (and a final charge state), sensing beyond this time a static HFI. The quantitative results obtained with this perturbation factor were in excellent agreement with the results of *ab initio* calculations of the EFG as a function of the charge state of the impurity, which shows a peculiar behavior close to the Fermi level, given strong support from first principles to the proposed AE scenario in ^{111}In-doped SnO_2. The experimental EFGs of these two time-dependent HFIs correspond to different final electronic configurations in which the double acceptor level introduced by the ^{111}Cd impurity is fully ionized or almost filled, respectively. Considering these important results and that TDPAC experiments using (a) ^{111m}Cd $\rightarrow$ ^{111}Cd as probe (in which the decay is not through an EC) in In_2O_3 [11,15], A-La_2O_3 [14], α-Al_2O_3 [16], Y_2O_3, and Sc_2O_3 [13], and (b) ^{111}In $\rightarrow$ ^{111}Cd in oxides deposited onto a metal substrate or codoped with donor impurities that can compensate acceptors [11,15] did not show this phenomenon, Darriba *et al.* [7] concluded that the ^{111}In EC decay, the acceptor character of the ^{111}Cd impurity, and the insulating nature of the host are shown to contribute to the existence of this type of time-dependent HFI in SnO_2, as well as in the other mentioned ^{111}In-doped binary oxides.

One of the central motivations of this paper is to elucidate the general conditions that the impurity-host system must satisfy to produce detectable time-dependent HFIs such as, e.g., the presence of EC decay of the probe of the parent, the acceptor character of the impurity probe, the values of the characteristic times involved in its γ-γ cascade, and the EFG dependence at the probe site with the ionization state of the impurity-host system. For this, we have selected to investigate in this paper the (^{111}In $\rightarrow$) ^{111}Cd-doped SnO semiconductor. This enables us to study a Cd-doped system where the Cd impurity should not introduce an acceptor level since Cd is isovalent to Sn in SnO.

Hence, in this paper, we report results combining TDPAC experiments at highly diluted (ppm) ^{111}In($\rightarrow$ ^{111}Cd) doping high purity polycrystalline SnO in a wide reversible measurement temperature range (20–900 K) and a complete *ab initio* electronic structure study of the Cd-doped system as a function of the fractional charge state of the supercell (SC). The calculations were performed using the full-potential augmented plane wave plus local orbitals (FP-APW + lo) method in large enough SCs to guarantee total convergence of the hyperfine parameters for all the studied charge states to correctly model the experimental impurity dilution. Also, defect formation energy calculations from first principles were performed to evaluate the relative probability of the different charge states of the Cd-doped system studied and to give support to the *ab initio* model presented for ^{111}In($\rightarrow$ ^{111}Cd)-doped SnO_2 [7].

The second principal motivation of this combined study arises from the controversial EFG characterization and its theoretical prediction from first principles at substitutional ^{111}Cd sites in SnO. Results were reported by Rentería *et al.* [29], performing a series of TDPAC experiments in ^{111}In($\rightarrow$ ^{111}Cd)-implanted Sn-O thin films that underwent different thermal treatments in air before each measurement at RT. The authors found that two oxidation states of Sn (2+ and 4+) initially coexisted, related with disordered SnO and SnO_2 phases that were transformed into crystalline SnO_2 by appropriate annealings. Since different phases coexisted in the sample, several interactions were necessary to reproduce the spectra, one of them being assigned to ^{111}Cd replacing Sn in SnO, characterized by $V_{33} = 8.2(3) \times 10^{21}$ V/m^2 (V_{33}, the largest component of the diagonalized EFG tensor) and a null asymmetry parameter η. This interaction appeared for a narrow window of annealing conditions and contributed to only 10% of the spectra, V_{33} being rather distributed. These spectra, always obtained at RT, were strongly dampened. This could be

due certainly to the presence of dynamic HFIs (at least coming from the SnO_2 phase), but the temperature dependence of the spectra was not measured, and this effect was not studied. Under these circumstances, it is impossible to guarantee this HFI assignment, a theoretical prediction for the EFG being of great help. Considering this, *ab initio* calculations in a $2 \times 2 \times 2$ SC were reported by Errico *et al.* [30]. In their study, using the FP-LAPW method, the dependence of the EFG for only three charge states of the SC was investigated by (a) replacing a Sn atom by a Cd one ($SnO : Cd^0$), (b) removing one electron from this Cd-doped SC ($SnO : Cd^{1+}$), and (c) adding one electron to the SC used in case (a) ($SnO : Cd^{1-}$). None of the V_{33} predicted for these charge states of the SC ($+6.2$, $+10.4$, and $-4.3 \times 10^{21}\,V/m^2$, respectively) agree with the experimental V_{33} reported in Ref. [29]. Due to this disagreement and the fact that the experiment of Ref. [29] was not designed to characterize ^{111}Cd atoms localized at defect-free cation sites in crystalline SnO, Muñoz *et al.* [31] performed TDPAC experiments in ^{111}In($\rightarrow$ ^{111}Cd)-diffused SnO polycrystalline powder pellets in the temperature range 295–900 K. Two clearly resolved HFIs (characterized at 295 K by $V_{33} = 5.7(9)$ and $8(1) \times 10^{21}\,V/m^2$) were necessary to reproduce the spectra in the whole temperature range. Their populations were constant in this range, and both interactions were characterized by rather low-asymmetry parameters tending to zero at high temperatures, in agreement with the coordination symmetry of the cationic site in SnO. A remarkable dampening of the spectra was observed <600 K. This effect was assigned to the presence of AE attributed to the EC decay of ^{111}In (EC) $\rightarrow$ ^{111}Cd. Unfortunately, the fitting routine used in Ref. [31] constrained the application of a unique time-dependent perturbation factor for all the interactions and with the same fitted dynamic parameters for each one. The more adequate analysis of the time-dependent HFI using independent dynamic parameters for each interaction done in this paper will have crucial implications for the correct modeling of the phenomena involved. It is worth mentioning that, in ^{111}Cd-doped SnO, only one HFI is expected for a complete substitutional localization of probes at the inequivalent cation site of the crystal structure. Since instead two HFIs were observed by Muñoz *et al.* [31], this fact could reflect the presence of two charge states of the ^{111}Cd atoms, a phenomenon recently observed in ^{111}In-doped SnO_2 [7].

The comparison of these TDPAC results with the *ab initio* calculations reported in Ref. [30] was not conclusive [31]. The disagreement between experiments and predictions may be because the correct modeling of the isolated character of the probe impurity has not been achieved.

In summary, for all these reasons, it is essential to study in detail, (a) from the experimental side, the behavior of the HFIs observed by Muñoz *et al.* [31] in a wider temperature range of measurement, down to 20 K, and to analyze in detail the spectra applying the time-dependent perturbation factor [7] for each interaction independently; (b) from first principles, the EFG behavior as a function of fractional charge states of the Cd-doped SnO SCs, the correct modeling of the Cd atom as an isolated impurity for all the charge states studied, and finally, the defect formation energies.

In what follows, in Sec. II, we present the TDPAC spectroscopy, the data reduction, and the time-dependent perturbation factor used to analyze the spectra; also, the sample preparation and the experimental results as a function of temperature are described. In Sec. III, the *ab initio* procedure is introduced, and we present and discuss the theoretical predictions for the structural and electronic properties, the EFG tensors, and the impurity formation energies for all the charge states studied. In Sec. IV, we compare and discuss the experimental and *ab initio* results, supporting the scenario proposed for the decay AE, and the conditions needed to observe this type of dynamic interactions in TDPAC experiments. Finally, in Sec. V, we present our conclusions.

II. EXPERIMENTAL SECTION

A. TDPAC spectroscopy and data reduction

The TDPAC technique determines the influence of extranuclear fields on the angular correlation between the directions of two successive γ rays (γ_1 and γ_2) emitted in a cascade during the nuclear decay of the probe atom. A description of the method as well as details about the TDPAC measurements can be found elsewhere [32–34]. Here, the well-known γ-γ cascade (171–245 keV) of the ^{111}Cd radionuclide, produced after the EC nuclear decay of the ^{111}In isotope, was used for the TDPAC measurements. The sensitive intermediate 245 keV nuclear state of this cascade has spin $I = +\frac{5}{2}$ and half-life $\tau_{1/2} = 84.1$ ns.

In this kind of experiment, we measure the number of coincidences $C(\Theta, t)$ where the second γ ray of the γ_1-γ_2 cascade is detected after a time t of the γ_1 emission, at an angle Θ with respect to the direction of γ_1. In our experiment, we have $\Theta = 90^\circ$ and 180°. Hence, the $R(t)$ TDPAC spectrum (the experimental spin-rotation curve) can be constructed as [35]

$$R(t) = 2\frac{C(180^\circ) - C(90^\circ)}{C(180^\circ) + 2C(90^\circ)} \cong A_{22}^{\exp} G_{22}^{\exp}(t), \qquad (1)$$

where $A_{22}^{\exp}$ is the experimental anisotropy of the γ_1-γ_2 cascade and $G_{22}^{\exp}(t)$ the theoretical perturbation factor $G_{22}(t)$ convoluted by the time-resolution curve of the spectrometer.

The time-dependent HFIs presented in this paper were analyzed in the framework of the model proposed by Bäverstam *et al.* [18] (BO). One of the advantages of the BO model, compared with other proposals (see Ref. [6]), is that it leads to a simple final analytical expression of the $R(t)$, allowing fitting to the experimental spectra. A detailed description of this model and an updated interpretation of the physical scenario behind this perturbation factor can be found in Ref. [7].

In the BO scenario, the on-off character of the observed dynamic HFIs is considered. This characteristic is related to the probability of the excited probe atom to decay to a certain stable electronic state, during the time window of the TDPAC measurement, leading to a final static electronic configuration. In this time window, transitions can occur among all the potential charge states of the probe atom, including the final stable charge state. Due to the transition between these different electronic configurations of the probe atom and its environment, the probe senses a fluctuating EFG until it reaches the final static EFG.

Within this model, to fit the $R(t)$ spectra, we use a perturbation factor that combines the dynamic and static

interactions as

$$G_{22}(t) = \left\{ \frac{\lambda_r}{\lambda_r + \lambda_g} \exp\left[-(\lambda_r + \lambda_g)t\right] + \frac{\lambda_g}{\lambda_r + \lambda_g} \right\} G^s_{22}(t)$$
$$= \{ f_d \exp\left[-(\lambda_r + \lambda_g)t\right] + f_s \} G^s_{22}(t), \quad (2)$$

where λ_r is the Abragam and Pound [36] relaxation constant, which measures the damping strength of the pure dynamic interaction related with the transitions among different probe charge states. The $\lambda_g = 1/\tau_g$ parameter is the atomic recovery constant, with τ_g the decay time of the recovery process of the probe atom which governs the on-off time of the dynamic interaction. Here, f_d and f_s can be thought of, in a different scenario [7], as the fractions of probes sensing all the time a dynamic or static HFI, respectively.

The $G^s_{22}(t)$ in Eq. (2) is the static perturbation factor commonly used in the case of static (time-independent) electric-quadrupole interactions, i.e., when the electronic environment of the probe nucleus does not change during the time interval defined by the emissions of γ_1 and γ_2. For polycrystalline samples and spin $I = +\frac{5}{2}$ of the intermediate nuclear probe state, $G^s_{22}(t)$ is written as

$$G^s_{22}(t) = S_{20} + \sum_{n=1}^{3} S_{2n}(\eta) \cos[\omega_n(\eta)t] \exp(-\delta\omega_n t). \quad (3)$$

The interaction frequencies ω_n and the coefficients S_{2n} are known functions [37] of the asymmetry parameter η. These frequencies are proportional to the nuclear quadrupole interaction frequency ω_Q, which in this case is related to the largest component of the diagonalized EFG tensor V_{33} by $\omega_Q = eQV_{33}/40\hbar$ [35], where Q is the nuclear quadrupole moment of the intermediate state of the probe. To obtain V_{33} from this relation, we use $Q = +0.83$ (13) b [38]. The δ parameter accounts for the statistical distribution around the fitted ω_n value originated, for a real sample, in slight differences in the environments of the probe.

In case the probe atoms in a sample are localized at different environments, e.g., at nonequivalent cation sites of a crystal structure, Eqs. (1) and (2) need to be modified accordingly using the usual static perturbation factor for multiple-site electric-quadrupole interactions:

$$R(t) \cong A^{\exp}_{22} G^{\exp}_{22}(t) = A^{\exp}_{22} \sum_i f_i G^{\exp}_{22_i}(t) = A^{\exp}_{22} \sum_i f_i \left\{ \frac{\lambda_{r_i}}{\lambda_{r_i} + \lambda_{g_i}} \exp\left[-(\lambda_{r_i} + \lambda_{g_i})t\right] + \frac{\lambda_{g_i}}{\lambda_{r_i} + \lambda_{g_i}} \right\} G^{s\ \exp}_{22_i}(t), \quad (4)$$

where f_i is the fraction of nuclei that senses each time-dependent HFI. In case one of these fractions senses a static HFI, the fitted λ_{r_i} will be zero.

B. Sample preparation and TDPAC measurements

The sample was prepared using high-purity SnO polycrystalline powder (Sigma-Aldrich 99.999%) pressed in a circular pellet of 5 mm diameter at 3×10^8 Pa and sintered at 1073 K to improve its crystallinity. To dope the ^{111}In($\rightarrow$ ^{111}Cd) tracers into the sample, 5 μL of a solution obtained dissolving 10 μCi of ^{111}In Cl_3 in 0.05 normal HCl solution in water was dropped onto the pellet and dried under infrared light. Then the activity was thermally diffused in vacuum atmosphere (7.5×10^{-6} Torr) slowly increasing the temperature up to 900 K and keeping it fixed at 900 K for 4 h.

The TDPAC spectrometer is based on four BaF_2 conical scintillators detectors, positioned 90° between them in a coplanar arrangement, with a slow-fast logic for the electronic setup. The $R(t)$ spectra were constructed from the 12 simultaneously recorded coincidence spectra $C(\Theta, t)$, four at $\Theta = 180°$ and eight at $\Theta = 90°$, using Eq. (1). The TDPAC measurements were carried out in the temperature range from 20 to 900 K in a reversible way.

For the high-temperature measurements, in the range from RT to 900 K, the sample was sealed in an evacuated quartz tube and placed into a small furnace with graphite electrodes centered between the four detectors. For the low-temperature measurements, in the range from 20 to 295 K, the sample was attached to the cold finger of a closed-cycle helium cryogenic device with temperature controlled to better than 0.1 K.

To be sure that only crystalline SnO is present in the TDPAC sample, i.e., that other tin oxide phases were not produced during the thermal treatments (as occurred in oxygen atmosphere, see Ref. [29]), the starting powder and the doped pellet (after the whole set of TDPAC measurements) were characterized by x-ray diffraction (XRD). In both cases, XRD results show all the lines corresponding to crystalline SnO, without evidence of SnO_2, the intermediate tin oxides (Sn_3O_4, Sn_5O_6), or metallic tin. In Fig. 1, we compare the x-ray diffractograms of the doped pellet after TDPAC measurements with the reference patterns of SnO_2 [39], Sn_3O_4 [40], Sn_5O_6 [41], and metallic Sn [42], in which the dashed lines represent the reference pattern of SnO [43].

C. TDPAC results

Selected representative $R(t)$ spectra and their corresponding Fourier transformations measured at $T = 20$, 150, 373, 500, 600, 700, 800, and 900 K are shown in Fig. 2.

In this figure, an increasing damping of the $R(t)$ signal is observed as the measuring temperature decreases from 900 to 20 K, this behavior being reversible with temperature. The shape of this damping is characterized by a strong decrease of the $R(t)$ signal in the first nanosecond (with respect to the A_{22} anisotropy at $t = 0$), keeping a surviving constant amplitude of the spectra after this initial strong damping. This characteristic shape agrees with the hypothesis based on the BO on-off model described in Sec. II A and presented in detail in Ref. [7]. Hence, we fit all the spectra with the perturbation factor presented in Eq. (4), which considers a time-dependent or a static ($\lambda_r = 0$) HFI solution for each interaction observed in the spectra.

In Fig. 2, the solid red lines are the best least-squares fits of Eq. (4) to the experimental $R(t)$ spectra (on the left) and the corresponding Fourier transformations of this $R(t)$

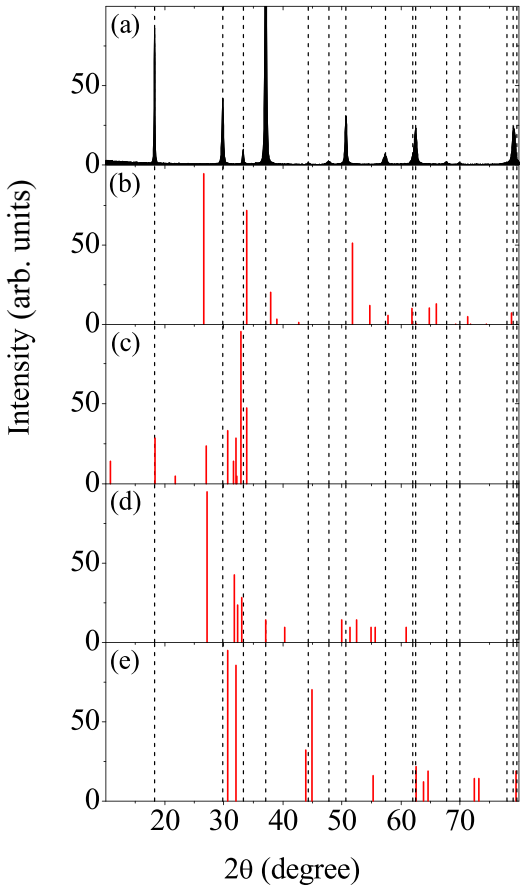

FIG. 1. Comparison between the x-ray diffractograms of the (a) doped pellet after time-differential perturbed γ-γ angular correlation (TDPAC) measurements with the reference patterns of (b) SnO_2 [39], (c) Sn_3O_4 [40], (d) Sn_5O_6 [41], and (e) metallic Sn [42]. In all pictures, the dashed lines represent the reference pattern of SnO [43].

fit (on the right). As shown in this figure, two HFIs (HFI1 and HFI2) were necessary to account for the $R(t)$ spectra along the entire temperature measurement range, as clearly seen in all the experimental Fourier spectra. The contributions of HFI1 and HFI2 are shown as shaded areas (in light blue and blue, respectively) in the Fourier spectra. HFI2, the minority one, is a well-defined static ($\lambda_r = 0$) HFI in all the temperature range. On the other hand, HFI1, the majority one, is a well-defined time-dependent HFI for all T, hence responsible for the increasing characteristic damping of the $R(t)$ spectra as temperature decreases. Figure 3 shows the more relevant hyperfine parameters obtained as a function of the measuring temperature. In this figure, when the error bars are not seen, the fitting errors are smaller than the data points. The whole set of spectra was fitted with a time-dependent perturbation function, the frequency distributions δ of HFI1 being fixed at high-temperature values, where the dynamic effect is very weak. The fractions of HFI1 and HFI2 are almost constant in the whole temperature range. Regarding the EFG tensor, from the temperature dependence of ω_Q and η, we observe that both parameters are approximately constant in the whole temperature range. In the case of the minority static HFI2, a subtle steplike behavior of ω_{Q_2} at

TABLE I. Experimental V_{33} and η obtained at the extreme measurement temperatures (20 and 900 K) for both HFIs.

Interaction	T (K)	V_{33} (10^{21} V/m^2)	η
HFI1	20	5.36(4)	0.29(2)
HFI2	20	7.34(5)	0.19(4)
HFI1	900	5.69(1)	0.10(1)
HFI2	900	6.78 (2)	0.06(3)

~600 K is present. This effect will be discussed in the next sections.

With respect to the time-dependent behavior of the spectra, HFI1 contributes with a strong dynamic character in the 20–700 K temperature range, as expressed by the increasing λ_{r_1} parameter as T decreases [also the small value of $\lambda_{g_1} <$ 700 K contributes to the damping of the spectra, see Fig. 3(b) and 3(c)], while HIF2 is static (i.e., $\lambda_{r_2} = 0$) in the whole temperature range. In this sense, Fig. 4 shows the relative weights of the dynamic and static terms of Eq. (2) for HFI1, where in the 20–900 K temperature range, this interaction does not achieve a pure static behavior.

Concerning the temperature dependence of λ_{g_1}, the steplike increase at 700 K means that the mean lifetime of the relaxation process (fast fluctuation among different electronic configurations of the ^{111}Cd atom) observed in the TDPAC measurement decreases. This is reflected in the high-temperature $R(t)$ spectra in which the static regime starts before (i.e., the off of the dynamic regime) than in the low-temperature spectra, leading to a constant amplitude pattern for higher times. On the other hand, as T decreases < 700 K, the off of the dynamic regime appears for larger times, reflected in the exponential decay of the $R(t)$ amplitude (see Fig. 2). For λ_{r_1}, it has its lowest values at high temperatures, leading to less dampened spectra.

In Table I, we summarize the obtained results for V_{33} and η at the extreme temperatures of 20 and 900 K. Comparing these results with those obtained in previous TDPAC experiments in the temperature range 295–900 K [31], we found that our values are in rather good agreement with those reported by Muñoz *et al.* [31] ($V_{33} = 5.7(9)$ and $8(1) \times 10^{21}$ V/m^2 at 295 K), but there are some important differences upon which to remark. Both HFIs found in their work were analyzed with the same time-dependent perturbation factor and the same dynamic parameters in the considered temperature range (due to constraints of the fitting code used at that time), while in this paper, we show that only HFI1 must be modeled with a dynamic HFI, whereas HFI2 has indeed a static character in the whole temperature range. The larger and less precise value found for HFI2 in Ref. [31] might have arisen from these fitting limitations.

III. *AB INITIO* CALCULATIONS

A. Calculation details

To enlighten the experimental TDPAC results, we performed electronic structure density functional theory (DFT)-based *ab initio* calculations in Cd-doped pristine SnO. Since the TDPAC samples employed here are doped with ^{111}Cd

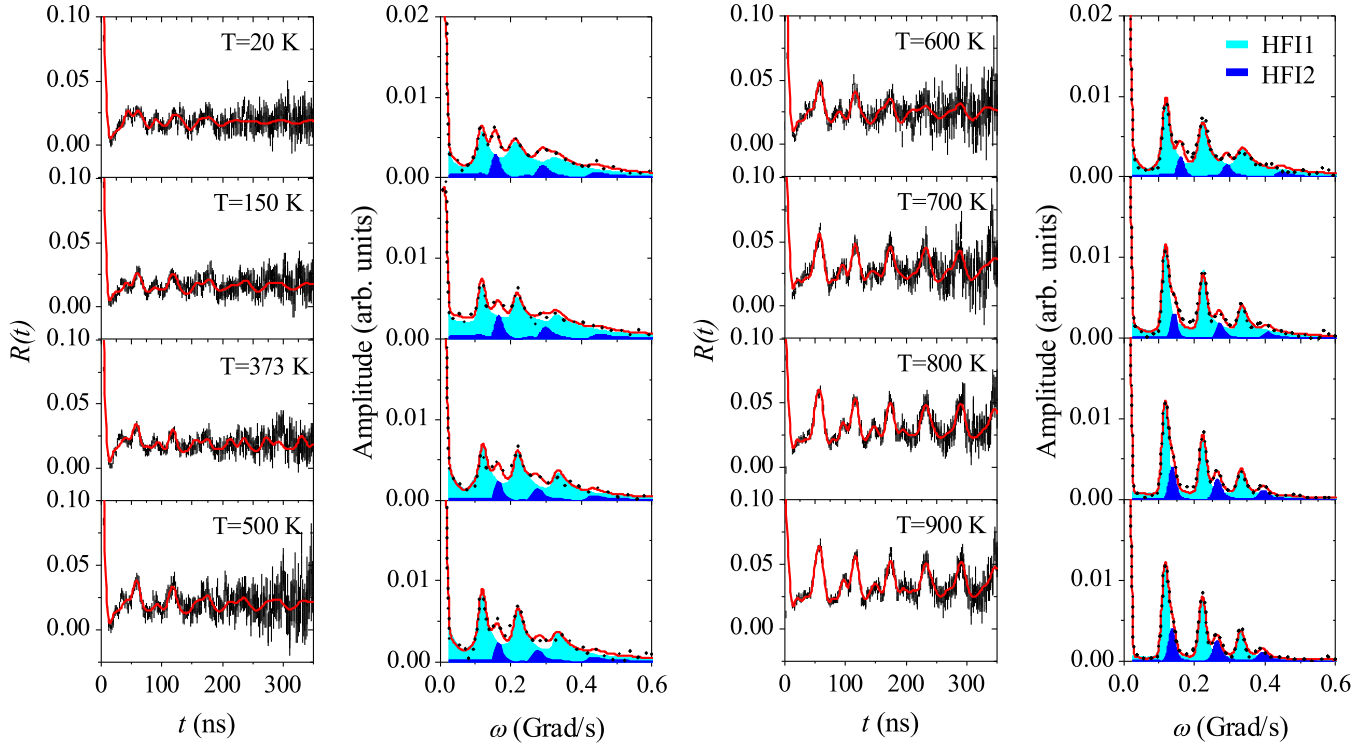

FIG. 2. $R(t)$ spectra (left) and their corresponding Fourier transformed spectra (right) taken at the indicated measuring temperatures.

atoms with ppm impurity dilution, we need to simulate an isolated Cd impurity, i.e., when each impurity does not interact with the nearest one and the structural relaxation induced by it on its neighbors do not affect the relaxations of the neighbors of the closest impurity. For this, we used a $3 \times 3 \times 3$ SC formed by 27 unit cells of SnO. Crystalline SnO is tetragonal, belonging to D^7_{4h} ($P4/nmm$) space group, with lattice parameters $a = b = 3.7986(1)$ Å and $c = 4.8408(2)$ Å [44]. The unit cell of this semiconductor contains two oxygen atoms at $2a$ positions (0, 0, 0) and ($\frac{1}{2}$, $\frac{1}{2}$, 0), and two tin atoms at $2c$ positions (0, $\frac{1}{2}$, v) and ($\frac{1}{2}$, 0, $-v$), with $v = 0.2369$ [44]. The structure has only one inequivalent cationic site and is made of layers where each Sn atom is at the apex of a square pyramid whose base is formed by its four nearest neighbor oxygen atoms (O_{NN}), as shown in Fig. 5(a). The $3 \times 3 \times 3$ SC is tetragonal, having lattice parameters $a' = 3a = b' = 3b = 11.399$ Å and $c' = 3c = 14.448$ Å, where one of the 54 Sn atoms is replaced by a Cd one (obtaining $Sn_{0.982}Cd_{0.018}O$), with a distance between nearest Cd atoms of ∼11.4 Å. We checked the convergence of the structural relaxations and the hyperfine parameters in other SCs, finding that the $3 \times 3 \times 3$ SC is sufficient to simulate an isolated Cd impurity, for all charge states of the SnO : Cd studied systems. Usually, this goal is achieved in doped oxides when the impurity-impurity shortest distance is ∼10 Å [7,22,25,27].

Here, Cd^{2+} is nominally an isovalent impurity in SnO, and the APW calculations reveal that the Sn substitution by a Cd atom (SnO : Cd^0) does not generate electronic holes (acceptor levels) in the valence band (VB). Nevertheless, the electronic relaxation process after the ^{111}In EC decay compels us to accurately predict the potential charge states of the doped system to describe its structural, electronic, and hyperfine properties correctly. Hence, we performed calculations for different charge states considering the partial filling of electronic states at the top of the VB (TVB), which are completely filled in the SnO : Cd^0 system, i.e., when a Cd atom replaces Sn in the SnO SC. For this, we removed the electronic charge from the doped SC in 0.1 e^- steps up to 1 e^- removed. Here, SnO : Cd^{q+} represents the system where a charge of q e^- is removed from the SnO : Cd^0 SC. In addition, we removed 2 e^- and added 1 e^- to the Cd-doped SC, calling these systems SnO : Cd^{2+} and SnO : Cd^{1-}, respectively.

All electron electronic structure *ab initio* calculations in the framework of DFT [45,46] were performed to determine the EFG tensor from an accurate description of the electronic density $\rho(\vec{r})$. The calculations were performed using the FP-APW + lo method [47], embodied in WIEN2K [48]. In this method, the wave functions are expanded in terms of spherical harmonics inside nonoverlapping spheres of radius R_{MT} centered at the atoms and in plane waves in the interstitial region. In all cases studied here, we take $R_{MT}(Sn) = R_{MT}(Cd) = 1.06$ Å and $R_{MT}(O) = 0.95$ Å. We found a cutoff parameter of the plane-wave bases of $R_{MT}K_{max} = 7$, necessary to warrant the convergence of the EFG for all charge states of the studied SC. Here, R_{MT} is the smallest radius of these nonoverlapping spheres, and K_{max} is the maximum modulus of the lattice vector in the reciprocal space. The integration in the reciprocal space was performed using the tetrahedron method [49], taking for the $3 \times 3 \times 3$ SCs a k-space grid of $3 \times 3 \times 3$. To obtain the equilibrium structure of the doped systems, they were relaxed, and each ion was displaced until the total force on it was below the tolerance value of 0.01 eV/Å. The EFG tensor was obtained from the second derivative of the full electronic potential [50,51].

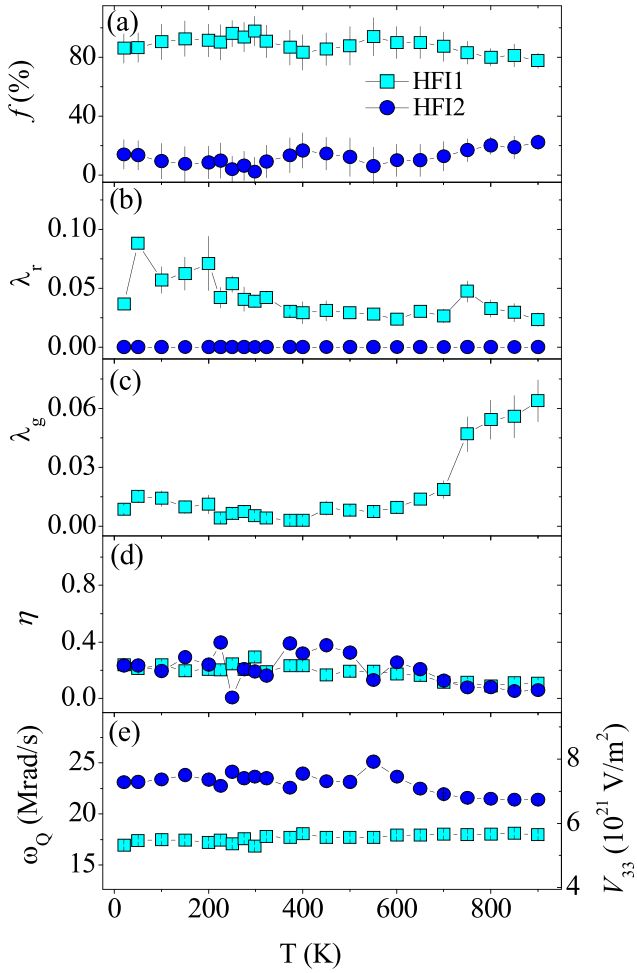

FIG. 3. Evolution of (a) fractions and (b)−(e) hyperfine parameters λ_r, λ_g, η, and ω_Q (or V_{33}), of both hyperfine interactions HFI1 and HFI2 as a function of the measurement temperature T.

We found for the converged $3 \times 3 \times 3$ SC that the Perdew-Burke-Ernzerhof and Wu and Cohen parametrization of the generalized gradient approximation of the exchange-correlation functional largely overestimates the structural relaxations, predicting very small EFGs, as was demonstrated in Ref. [30] for smaller SCs, in large disagreement with the

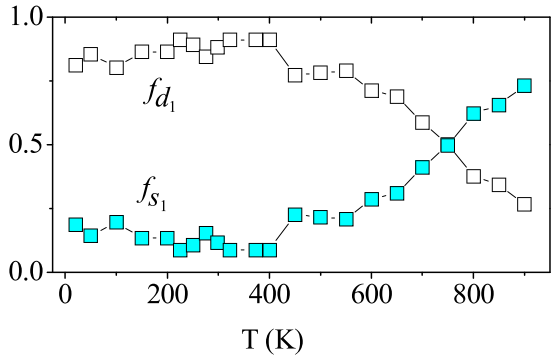

FIG. 4. f_d and f_s for HFI1, computed using Eq. (2) and the fitted λ_r and λ_g parameters shown in Figs. 3(b) and 3(c).

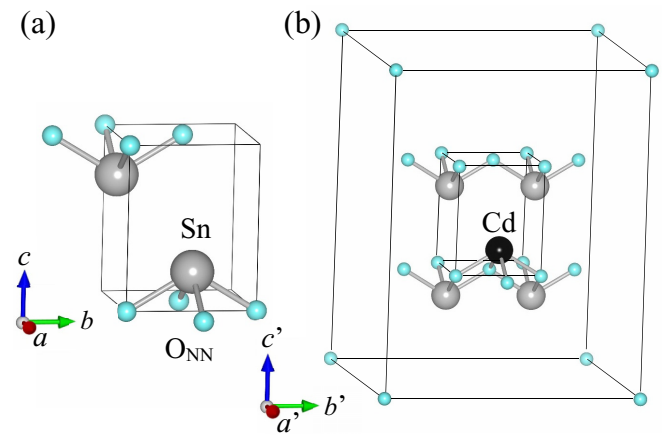

FIG. 5. (a) Tetragonal SnO unit cell. (b) Supercell with $a' = 3a$, $b' = 3b$, and $c' = 3c$. The gray, black, and light-blue spheres correspond to Sn, Cd, and O atoms, respectively.

experimental values. For this reason, all the theoretical results shown in this paper were obtained using the local density approximation functional to treat the exchange-correlation effects.

B. Calculations results

1. Impurity dilution

At a first step, as mentioned before, we studied the SC size effect to simulate an isolated Cd impurity in this oxide so that each impurity does not interact with the nearest ones and the structural relaxations of its neighbors do not affect the relaxations of other neighbors of the closest impurities. In this sense, we studied the convergence of the EFG tensor (the most sensible magnitude predicted in this paper by these *ab initio* calculations) as a function of the Cd impurity dilution, i.e., increasing the SC size for different charge states. We found that a $3 \times 3 \times 3$ SC is necessary to simulate the isolated Cd impurity for all the doped systems studied here. It is interesting to note that, only in the special case of the SnO : Cd^0 system, i.e., the system in which the Fermi level resulted located at the TVB, a $2 \times 2 \times 2$ SC is already sufficient to guarantee the isolated condition of the impurity, resulting as a necessary methodological general rule to check the correct dilution for charged systems too.

2. Structural relaxations

In Fig. 6, we sketch the relaxation process at the Cd impurity site. For the SnO : Cd^0 and SnO : Cd^{1+} systems, the Cd atom moves down only along the c axis toward the O_{NN}, and these atoms relax outward basically in the a-b plane. The equivalent O_{NN} atoms labeled O_a (O_b) are distributed parallel to the a (b) axis and move along this axis, respectively. The Cd-O_{NN} bond length (d_{Cd-ONN}) increases from 2.220 to 2.268 Å for the SnO : Cd^0. When an electron is removed, this bond length relaxes up to 2.256 Å. In this case, the Cd atom moves down four times the distance it moves in the SnO : Cd^0 system, and the O_{NN} relax again a little longer [Fig. 6(a)]. The shorter relaxed bond length achieved agrees with a Coulombic attraction of the O_{NN} when the negative

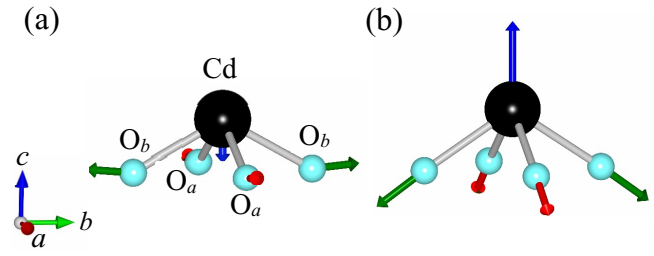

FIG. 6. Final positions of Cd and O_{NN} atoms after the full structural relaxation for (a) SnO : Cd^{1+} and (b) SnO : Cd^{1-} systems. Each arrow length is proportional to each atom displacement. In (a), red and green colors indicate that the oxygen displacement is practically parallel to the *a* and *b* axes. In (b), these displacements are in the Cd-O_{NN} bond direction. The Cd atom only moves in the *c* direction in both cases.

charge is removed from the Cd atom. The same happens when a fractional charge is removed from the SC. On the other hand, for the SnO : Cd^{1-} system, the Cd atom moves up along the *c* axis 10 times the distance it moves in the SnO : Cd^0 system, while the O_{NN} atoms relax outward along the Cd-O_{NN} bond directions, as shown in Fig. 6(b), enlarging the final Cd-O_{NN} distance (2.363 Å), in agreement with a Coulombic repulsion.

3. Electronic structure

When a Cd impurity atom replaces a Sn atom in SnO, it introduces atomic impurity levels in the density of electronic states (DOS) at the bottom of the VB (BVB), mainly with *d* character, and a distribution of a low number of Cd states (mixture of *d* and *p* states) that tends to an almost flat negligible distribution of states at the TVB. At the same time, the Cd atom introduces an impurity level at the bottom of the conduction band (BCB) that is also a mixture of *d* and *p* states, this level being empty in the SnO : Cd^0 system, as shown in Fig. 7. The effect of removing one electron from the SnO : Cd^0 system on the different Cd *p* and *d* orbitals near the Fermi level is shown in Fig. 8, showing a rigid bandlike behavior whose effect will be discussed during the analysis of the EFG at the Cd site.

Comparing the DOS shown in Fig. 7(a) with that corresponding to the 2 × 2 × 2 SC (see Fig. 2(b) in Ref. [30]), we see that, in the last one, the Cd atom introduces an additional impurity level at the TVB, which is completely filled in the SnO : Cd^0 system. As we mentioned before at the beginning of this subsection, we need a 3 × 3 × 3 SC to simulate the isolated Cd impurity for the different charged states studied in this paper. In the special case of the SnO : Cd^0 system, the EFG is already converged for the 2 × 2 × 2 SC; however, the isolated impurity character is not achieved. The reason of this strange behavior is that the appearance of this spurious peak in the 2 × 2 × 2 SC, which is due to the closeness of the Cd impurities and is mainly of p_z character, does not change the relative weight the Cd-p_x, Cd-p_y, and Cd-p_z states have in the converged 3 × 3 × 3 SC along the VB [Fig. 8(a)], thus not changing the EFG. On the other hand, when an electron is removed from the SC, the EFG increases with respect to that of the SnO : Cd^0 system, but the change in the 2 × 2 × 2 is twice the change in the converged 3 × 3 × 3 SC. In these

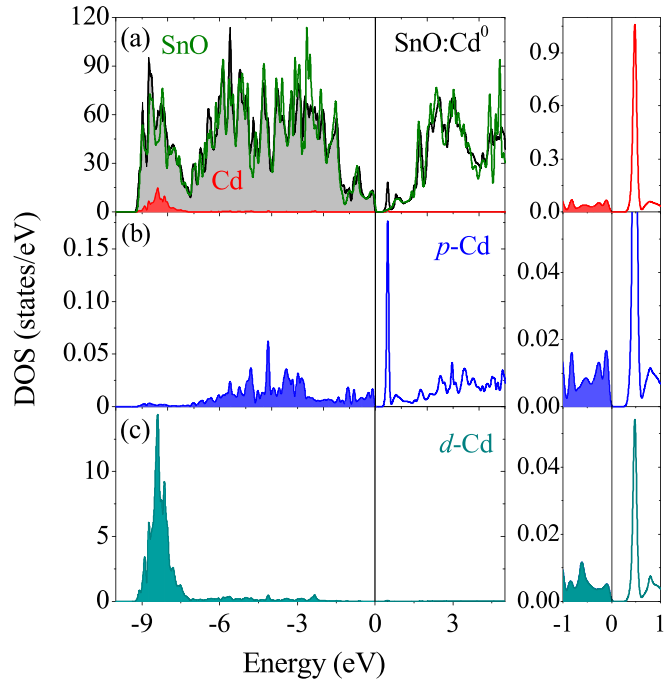

FIG. 7. (a) On the left, total density of electronic states (DOS) for SnO (green line), SnO : Cd^0 (black line) and the Cd contribution (red line). On the right, the Cd contribution is augmented two orders of magnitude for energies close to the Fermi level, set as 0 eV (vertical line). (b) and (c) *p*- and *d*-Cd partial DOS (PDOS) for SnO : Cd^0, respectively. On the right, these PDOSs are augmented for energies close to the Fermi level. The shaded areas represent filled valence band electronic states.

cases, the relative weight of the Cd-*p* states changes more abruptly as the negative charge is removed from the 2 × 2 × 2 SC than in the 3 × 3 × 3 SC [Fig. 8(b)].

4. EFG

To investigate a possible EFG tensor dependence with the charge state of the SC that could be at the origin of the dynamic HFIs and to try to correlate these predictions with the experimental EFGs that characterize the two HFIs observed in our TDPAC experiments, we performed EFG calculations at Cd sites in Cd-doped SnO as a function of the charge state of the SCs. In Table II, we show the EFG tensor predictions calculated for the SnO : Cd^0, SnO : Cd^{1+}, SnO : Cd^{2+}, and SnO : Cd^{1-} systems after the full structural relaxation. First, the V_{33} direction results parallel to the $c = [0\ 0\ 1]$ crystal axis, and the null asymmetry parameter is consistent with the axial

TABLE II. V_{33}, η, and V_{33} direction predicted for SnO : Cd^0, SnO : Cd^{1+}, SnO : Cd^{2+}, and SnO : Cd^{1-} SCs.

	V_{33} (10^{21} V/m^2)	η	V_{33} direction
SnO : Cd^0	+5.30	0.0	[001]
SnO : Cd^{1+}	+7.49	0.0	[001]
SnO : Cd^{2+}	+8.45	0.0	[001]
SnO : Cd^{1-}	−3.43	0.0	[001]

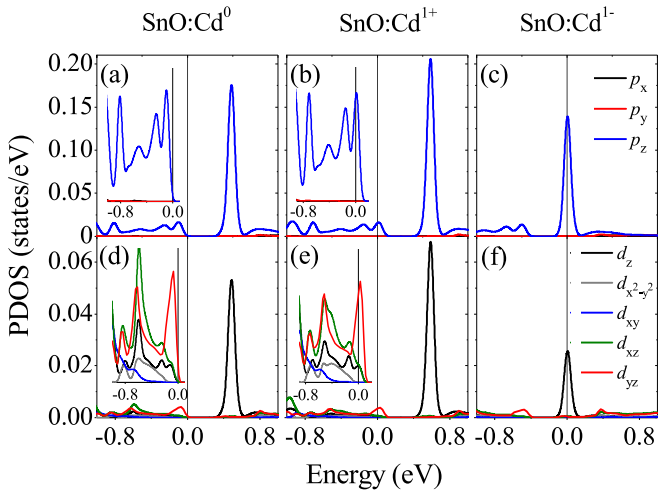

FIG. 8. p-Cd (up) and d-Cd (bottom) partial density of states (PDOS) for the SnO : Cd^0 (left), SnO : Cd^{1+} (middle) and SnO : Cd^{1-} (right) systems. The energy is referred to the Fermi level (vertical line). x, y, and z directions of the p- and d-Cd PDOS are coincident with the a, b, and c unit cell vectors. The insert in each picture corresponds to a zoom near the Fermi level.

symmetry of the cation site (see Fig. 5) for all the charge states of the SCs studied. These characteristics of the EFG tensor do not change with respect to pure SnO. Second, V_{33} indeed strongly depends on the charge state of the Cd impurity, increasing its positive value when 1 or 2 electrons are removed and decreasing to negative values when 1 electron is added to the SC.

To understand this dependence, in Fig. 9(a), we show the total V_{33} and their p and d contributions as a function of the charge states of all the SCs studied. The negative charge removed from 0 to 1 electron in 0.1 e^- steps is zoomed in Fig. 9(b). As can be seen, the strong V_{33} variation is governed by the p contribution, d being almost independent from the charge state of the SC. For the system SnO : Cd^0, the p and d contributions to V_{33} (V_{33}^p and V_{33}^d) are almost equal, but when the system is positively charged, the p contribution increases and dominates. To understand this behavior from the Cd-p partial DOS (PDOS), it is necessary to introduce the asymmetry count Δn_p that is proportional to the p contribution to V_{33}:

$$\Delta n_p = \tfrac{1}{2}\left(n_{p_x} + n_{p_y}\right) - n_{p_z}, \tag{5}$$

where n_{p_i} is the occupation number of the corresponding p_i orbital. Each atom under consideration has its own xyz system to describe its orbitals. For the Cd atom, the z axis is in the c direction, while the x and y axes are parallel to a and b, respectively. Inspecting this figure, when negative charge is removed from the SC, the Fermi level moves to lower energies, depleting Cd-p_z orbitals [see Fig. 8(a)], hence increasing Δn_p and V_{33}^p. Nevertheless, this is strictly true in a rigid-band model. In effect, the changes in n_{p_i} along the entire VB must be considered. Doing this, the modifications in n_{p_x} and n_{p_y} also contribute to the increase of V_{33}^p. In effect, integration of the p_i PDOS along the VB gives a greater increase of V_{33}^p due to the increase of n_{p_x} and n_{p_y} relative to the decrease of

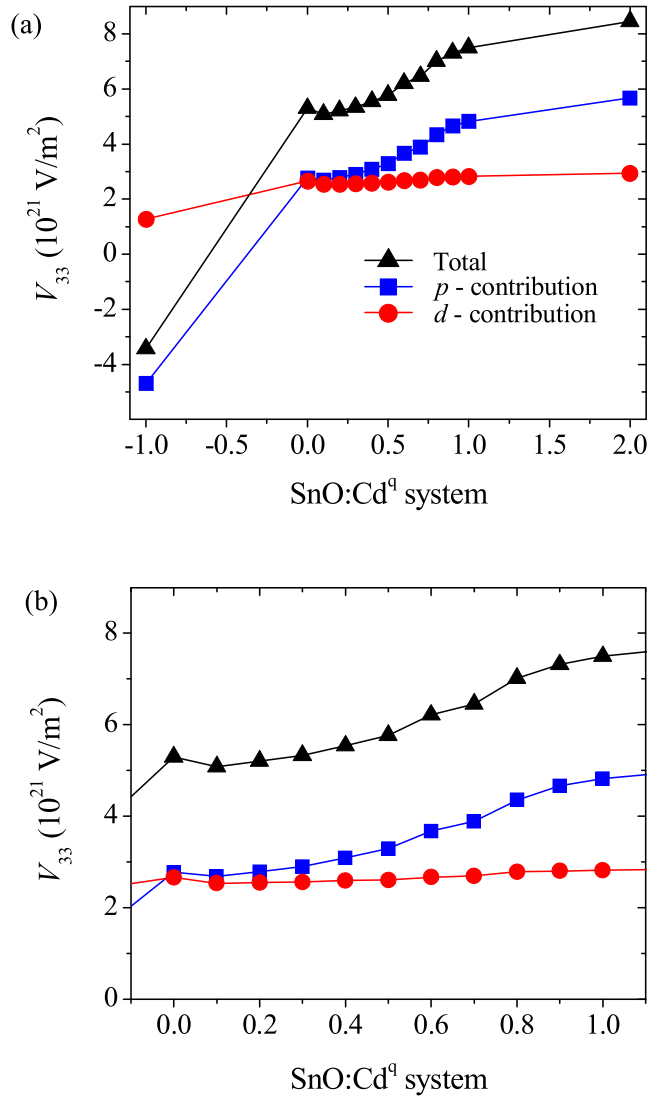

FIG. 9. (a) V_{33} (triangles), and its p (squares) and d (circles) contributions as a function of the negative charge added to and removed from the supercell (SC). (b) The same as in (a) but in the charge region from 0 to 1 electron removed from the SC.

n_{p_z}. In addition, the little decrease of V_{33} predicted when 0.1 electron is removed from the SC can be only explained by modifications of n_{p_i} along the whole VB, i.e., an increase of n_{p_z} and/or a decrease of n_{p_x} and n_{p_y}. In effect, what really happens is that n_{p_z} is almost constant, and n_{p_x} and n_{p_y} slightly decrease their value. In the same way, an analysis of the d orbitals shows that they contribute also with a slight decrease of V_{33}^d. On the other hand, if one electron is added to the SC, the impurity level at the BCB (which has mainly Cd-p_z and d_{z^2} symmetries) becomes partially filled. The increase of n_{p_z} strongly decreases V_{33}^p to negative values. In this case, we need to also analyze the d orbital contribution to V_{33}, through the asymmetry count:

$$\Delta n_d = \left(n_{d_{x^2-y^2}} + n_{d_{xy}}\right) - \left[\tfrac{1}{2}\left(n_{d_{xz}} + n_{d_{yz}}\right) + n_{d_{z^2}}\right]. \tag{6}$$

In this case, the increase of $n_{d_{z^2}}$ decreases V_{33}^d but in a much smaller extent (nine times with respect to the change in V_{33}^p),

without changing its sign. The behavior of the predicted V_{33} is also related to the structural relaxations described before (see Fig. 6) and the charge redistribution produced. When an electron is removed (added) from (to) the SC, the Cd-O_{NN} pyramid flattens (elongates), distributing more negative charge at the x-y plane (along the z axis) and producing a positive (negative) increment of V_{33} (whose direction is parallel to the $c = z$ axis) due to the angular dependence of the strength and sign of V_{ii} as a function of the angle of a negative charge (source) with respect to the V_{ii} direction (see eq. (14) in Ref. [7]).

To predict qualitatively the modification of the EFG when an electron is removed or added to the Cd-doped SC using reliable DFT calculations (in contrast to the procedure used in point-charge model predictions in which the oxygen positions matter), one must compute the EFG change due to the modification of the electronic charge density $\rho(\mathbf{r})$ inside the Cd muffin-tin sphere, particularly that very close to the Cd nucleus. In Fig. 10, we plotted electron densities localized in a plane parallel to the b-c plane containing the Cd impurity and two of its four O_{NN} atoms (those labeled as O_b in Fig. 6). Figure 10(a) shows the electron density of the occupied states in an energy range corresponding to the last electron below the Fermi level in the SnO : Cd^0 system. In a rigid-band model, this electronic charge is the one removed from the SC to obtain the SnO : Cd^{1+} system. Figures 10(a) and 10(b) compare those corresponding to SnO : Cd^0 and pure SnO, respectively. The substitution of a Sn atom by a Cd (isovalent) impurity in the SC, for this energy region at the TVB, tilts the orientation of the O_{NN} orbitals from their original alignment in the c direction, introduces rather disperse charge in all the SC (mainly in certain oxygen atoms far from the Cd atom), and localizes negative charge at the Cd site. The electronic charge that will be removed from the Cd atom to obtain the SnO : Cd^{1+} system is concentrated along the c axis, thus producing the predicted positive increase of V_{33} (removing negative charge from the z axis is qualitatively equivalent to adding negative charge in the x-y plane). In opposition to this behavior, when one electron is added to the SC to obtain the SnO : Cd^{1-} system, this charge is almost only localized at the Cd atom along the c axis and at its O_{NN} along a direction very close to the Cd-O_{NN} bonds, as shown in Fig. 10(c). The negative charge localized at the Cd atom pointing along the c axis and away from the O_{NN} atoms is responsible for the strong negative increment of V_{33} when one electron is added to the SC.

Up to now, in all oxide hosts studied by us with nominal acceptor Cd impurities, energetically localized empty impurity levels were observed to be introduced at the TVB. In all these cases, when one electron is added to the SC, it results in being localized at the Cd atom and its nearest neighbors. In this sense, it is worth noting that the added electron in SnO : Cd results in being localized at the Cd impurity. In effect, adding one electron to the SnO : Cd^0 SC partially fills the empty impurity level introduced at the BCB. This level is energetically very localized and has p_z-Cd character. However, contrary to this situation, the electron removed from the SnO : Cd^0 system is much more dispersed along all the atoms of the SC, as mentioned before. This effect correlates well with the fact that the Cd impurity introduces delocalized states at the TVB. In turn, this seems to be because Cd is nominally an isovalent impurity in SnO.

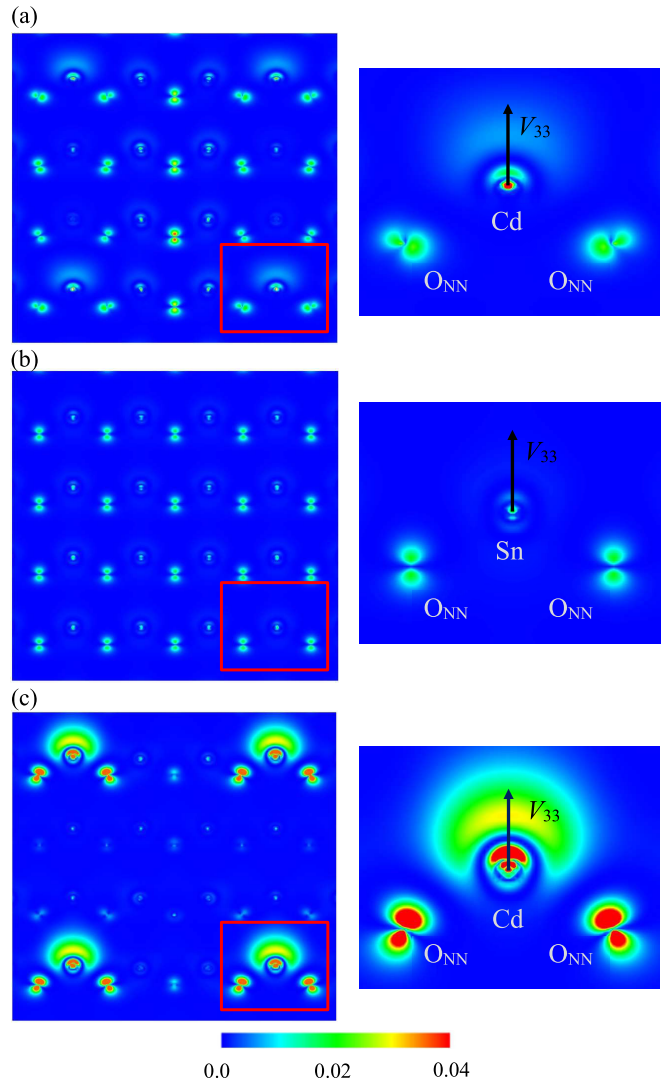

FIG. 10. Electron density in the energy range corresponding to the most energetic e^- below the Fermi energy for (a) SnO : Cd^0, (b) SnO, and (c) SnO : Cd^{1-}. On the right, a zoom of the SC region delimited by the red square is shown. In (a) and (c), the Cd impurities are the cations localized near the corners of each plane.

Based on what was said above, the general dependence of the EFG on the electronic charge distribution close to the probe nucleus explains the changes in V_{33} when adding or removing negative charge to the SC. Particularly, when an electron is removed from the SC (see Fig. 9), the fact that the final Cd-O_{NN} distances for this charged SC remain almost equal to that in the SnO : Cd^0 system (see Sec. III B 2) allows us to show the strong sensitivity of the EFG tensor at the Cd site to subtle local geometrical distortions related with the changes in the electronic distribution close to the Cd impurity.

5. Impurity formation energies

To unravel the different assignments of the experimentally observed HFIs to the different scenarios raised by the EFG predictions performed as a function of the charge state of

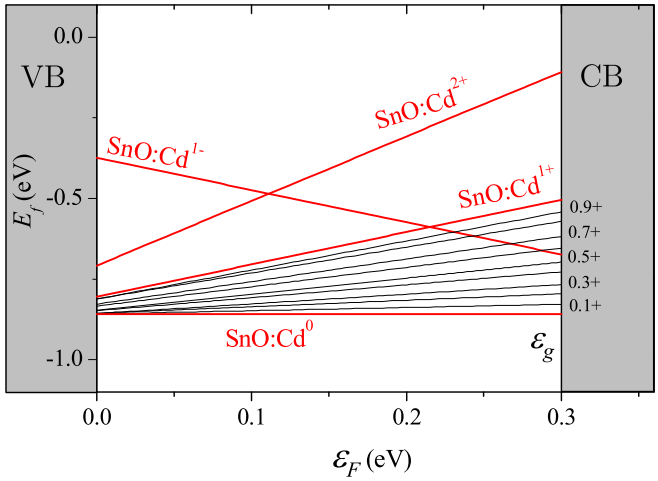

FIG. 11. Defect formation energy E_f as a function of the Fermi energy level ε_F for all SnO : Cd^q studied. Red lines correspond to $q = 1-$, 0, 1+, and 2+, whereas the black lines correspond to $q =$ 0.1+, 0.2+, 0.3+, 0.4+, 0.5+, 0.6+, 0.7+, 0.8+, and 0.9+. ε_g is the predicted bandgap energy. VB and CB represent schematically the valence and conduction band regions of the pure SnO, respectively.

the SC and to give support from *ab initio* calculations to the scenario proposed for the dynamic behavior, we performed energetic studies. The defect energy formation for Cd-doped SnO is given by

$$E_f^q = E^q(n_{\mathrm{Sn}}, n_{\mathrm{O}}, n_{\mathrm{Cd}}) - n_{\mathrm{Sn}}\mu_{\mathrm{Sn}} - n_{\mathrm{O}}\mu_{\mathrm{O}} - n_{\mathrm{Cd}}\mu_{\mathrm{Cd}} + q(\varepsilon_{\mathrm{F}} + \varepsilon_v'), \quad (7)$$

where $E^q(n_{\mathrm{Sn}}, n_{\mathrm{O}}, n_{\mathrm{Cd}})$ is the total energy of the doped SC in the charge state q, containing n_{Sn}, n_{O}, and n_{Cd} atoms of tin, oxygen, and cadmium, respectively, and μ_{Sn}, μ_{O}, and μ_{Cd} being their chemical potentials. Here, ε_{F} ($0 \leqslant \varepsilon_{\mathrm{F}} \leqslant \varepsilon_g$, where ε_g is the bandgap energy) is the Fermi energy relative to the energy of the TVB $\varepsilon_v' = \varepsilon_v + \delta_q$, where ε_v is the energy of the TVB of the pure system, and δ_q is a correction that lines up the band structure of the pure and doped bulk systems. Following the formalism presented in Ref. [22], we obtain the formation energy of a Cd impurity in a Sn substitutional site in SnO with a charge state q, considering an O-rich environment of the impurity as

$$E_f(\mathrm{SnO:Cd})^q = E(\mathrm{SnO:Cd})^q - E(\mathrm{SnO}) + \mu^*_{\mathrm{Sn}} + \Delta_f H^{\mathrm{SnO}} - \mu^*_{\mathrm{Cd}} - \Delta_f H^{\mathrm{CdO}} + q(\varepsilon_{\mathrm{F}} + \varepsilon_v'). \quad (8)$$

Here, $\Delta_f H$ are the formation enthalpies, and μ^* are the metallic crystal total energy per atom. The results for all charge states studied are shown in Fig. 11.

IV. DISCUSSION

A. Experimental and *ab initio* support to the ECAE scenario proposed

When the experimental results (Table I) are compared with the *ab initio* predictions (Fig. 9), we see that the systems that agree with the experimentally observed HFIs, HFI1 and HFI2, across all temperature ranges, are those generated in SCs with a charge state range of 0 to 1 electron removed, i.e., from 0 to 1 electronic hole. When we inspect closely at this charge state region, as shown in Fig. 9(b), we can see that the observed V_{33} and η values that characterize the time-dependent HFI1 in the temperature range 20–900 K correspond with those predicted for the SnO : Cd^q ($0 \leqslant q \leqslant 0.5$) SCs.

This excellent agreement, combined with the analysis of the defect formation energy calculations described in the preceding section, which shows that the SnO : Cd^0 system has the lowest formation energy, allows us to definitively assign HFI1 to ^{111}Cd probes localized at defect-free substitutional Sn sites (ionization state $q = 0$). On the other hand, the fact that the SnO : Cd^q systems ($0 \leqslant q \leqslant 1$) have very similar formation energies at the TVB and different EFGs predicted for these charge states supports from first principles the existence of random fluctuations between different EFGs, a necessary situation considered in the construction of the B-O on-off perturbation factor [7] used in this paper. It should be noted that the EFG fluctuation that contributes to the damping of the $R(t)$ spectra must come from fluctuations among charge states within the region from 0 to 1 electron removed (0–1 electronic holes), provided that the fluctuation includes at least one charge state between 0.5 and 1 electronic holes, because the EFG varies significantly in this region [see Fig. 9(b)]. We shall see in the next paragraphs why the dynamic regime of the EFGs should not emerge from a more expanded charge region (e.g., between 1 to 2 electronic holes).

The minority HFI2 interaction, which is static (i.e., time independent) across the temperature range of measurement, exhibits V_{33} and η values that are very close to those predicted by the SnO : Cd^{1+} system (one electronic hole added to the neutral SC). A deeper inspection at the HFI2 parameters at temperatures <600 K reveals that the charge state is, in fact, $q = 0.9+$. The defect formation energy investigation reveals that the system energy increases with increasing number of electronic holes when compared with the neutral (SnO : Cd^0) system (in which the VB is entirely filled), which is consistent with the presence of a low fraction of probes giving rise to HFI2. Both characteristics allow us to associate HFI2 with ^{111}Cd probes located at substitutional Sn sites with a trapped electronic hole (ionization state $q = 1+$). Because HFI2 is static at any temperature, any dynamic event occurs at the ^{111}Cd nucleus before the time window of the TDPAC measurement (i.e., before the γ_1 emission from the $I = \frac{7}{2} +$ 416 keV nuclear state, which has a lifetime of 1.2×10^{-10} s = 0.12 ns) [52].

Since HFI2 is static and originated in a $q = 1+$ state (one trapped electronic hole), it implies that the EFG fluctuations occur before the TDPAC time window, and when the measurement begins, only one electron hole remains unfilled at all probe atoms, including those that perceive HFI1. These EFG fluctuations are produced by the Auger electron cascade and the relaxation process, during which about seven holes are formed [8,53], diffused to the outer atomic shells of Cd, and neutralized by diffusion in the VB. Because SnO is a *p*-type semiconductor, owing mostly to the existence of Sn vacancies, these acceptor states compete for electrons with the electronic holes trapped at Cd atoms. Since the Cd atoms are at ultralow ppm concentrations and its trapped hole is delocalized along the crystal lattice, negative charge from distant sources would

fill the acceptor centers and the delocalized hole before filling the fraction of holes localized at the Cd atom. During the TDPAC time window, most of the probes (those that sense HFI1) attempt to reach the neutral ground state, filling this hole, while a small number of probes (those that sense HFI2) remains with the hole unfilled due to the extremely low electron availability. Most Cd probes that experience a time-dependent interaction (HFI1) attain (slowly) their final neutral charge state ($q = 0$), revealing the dynamic regime for a few nanoseconds before this final state (the off). This is also consistent with the limited carrier mobility of SnO [54]. In this scenario, it is evident why the dynamic regime in SnO cannot be caused by fluctuations between charge states greater than $q = 1+$, for example, between 1+ and 2+, because all probes have only one trapped electron hole. This is also qualitatively consistent with the bigger difference in energy formation between $q = 1+$ and 2+ at the TVB.

For temperatures <600 K, HFI2 was perfectly represented by Cd atoms in the SnO : Cd^{1+} SC, as previously stated. Here, V_{33_2} drops at higher temperatures to values consistent with those anticipated by SnO : Cd^q, with q between 0.7+ and 0.8+ [see Fig. 9(b)]. At these higher temperatures, the minority Cd probes (HFI2) attempt to fill more holes (decrease system energy), allowing them to return to this lower charge state ($q = 0.7+$) in a shorter time than the TDPAC time window (always giving a static interaction). Simultaneously, most probes (HFI1) reduce the lifetime of their electronic holes (λ_g suddenly increases for $T > 600$ K), resulting in less dampening of the $R(t)$ spectra as temperature increases for $T > 600$ K. Both facts agree with the increase of one order of magnitude in the electron availability (between 600 and 900 K) owing to intrinsic ionization of the semiconductor $n(T)$ [55], which increases carrier density (the mobility does not increase with T).

Finally, we wish to compare the time-dependent HFI results in (^{111}In →) ^{111}Cd-doped SnO_2 as a function of temperature [7] with the SnO results provided here. As stated in the introduction, two time-dependent HFIs were found in SnO_2 : ^{111}Cd, corresponding to a final electronic configuration in which the double acceptor level produced by the Cd impurity is fully ionized (named HFI1) or almost filled (HFI2). Both interactions became static ($\lambda_r = 0$) at temperatures >650 and 923 K, respectively, increasing the population of HFI1 at the expense of the population of HFI2. Because of the natural occurrence of oxygen vacancies, SnO_2 is an n-type semiconductor with a high free-electron carrier concentration. In addition, it has greater carrier mobility than SnO. These properties might explain the absence of a static HFI over the whole temperature range of measurement (as seen with HFI2 in SnO); the carrier concentration in SnO_2 at low and medium temperatures is sufficient to ionize the double acceptor impurity level within the TDPAC time window. The intrinsic ionization effect $n(T)$ [55] raises the carrier concentration by six orders of magnitude (from 5×10^4 to 1×10^{10} electrons/cm^3) as T increases. The large increase in electron availability in SnO_2 can explain the complete ionization of the double acceptor level before the TDPAC time window (HFI1 transforms to a static regime) and the decreasing fraction of HFI2 and its transformation to a static HFI until its disappearance.

B. Origin of the observation of this type of time-dependent HFI in TDPAC probes

The information obtained here on the static HFI2 in SnO allows us to gain a perspective on the origin of the dynamic ECAE phenomenon. Before the emission of γ_1, a minority fraction of probes (sensed by HFI2) reaches a stable electronic configuration, filling all the electronic holes created by the EC and the Auger process except the outermost one. We suppose that all the ^{111}Cd probes fill all the holes, except one, at the same time and in the same way. On the other hand, most probes (as detected by HFI1) fill this last hole following the emission of γ_1, resulting in the dynamic interaction, with the latter effect depending on temperature and the electron availability of the host. This crucial information allowed us to calculate the number of electronic holes involved in the generation of the dynamic effect, only one in the case of SnO : ^{111}In, assuming that the off of the charge state fluctuation of the probe (and the EFG fluctuation) occurs after the emission of γ_1. In other words, the emission of γ_1 must be fast enough in comparison with the recovery time of this electronic hole. The nuclear level that decays emitting γ_1, $\tau_{1/2}(\gamma_1) = 0.12$ ns, in [^{111}In (EC) →]^{111}Cd meets this criterion [7–17]. It should be noted that the apparent lack of this type of dynamic interaction in ^{111}In(→ ^{111}Cd)-doped TiO_2 [56,57] is not completely conclusive. The employment of a silver sample container in Ref. [57] and the sol-gel procedure in Ref. [56] may have nullified its observation. The effect of the sol-gel procedure on these dynamic HFIs was studied by Richard *et al.* [58]. The [^{99}Rh (EC) →]^{99}Ru and [^{100}Pd (EC) →]^{100}Rh probes, have $\tau_{1/2}(\gamma_1) = 1.04$ ns and $\tau_{1/2}(\gamma_1) = 0.35$ ns, respectively, resulting in dynamic HFI when doping insulators [59]. In this regard, the absence of dynamic HFI in TDPAC studies in ^{44}Ti[(EC) → ^{44}Sc]-doped TiO_2 offered evidence. The ^{44}Sc probe is formed by an EC decay in this situation, and it is an acceptor in this host; however, the $\tau_{1/2}(\gamma_1) = 51.1\ \mu$s is far longer than the average electronic hole recovery time; thus, the dynamic interaction cannot be detected [60].

In ^{111m}Cd, however, $\tau_{1/2}(\gamma_1) = 48.6$ min, after which the TDPAC measurement begins. This is a very long time in comparison with the electronic recovery time of the last hole in SnO, which is only a few tens of nanoseconds. The lack of this type of time-dependent HFI in TDPAC experiments in different binary oxides [13–16] using the ^{111m}Cd probe impurity, which does not decay through EC and thus does not produce extra electronic holes at the ^{111}Cd atom (aside from the acceptor level introduced by the Cd impurity itself), has led to the conclusion [7,14] that the acceptor character of the probe is not a sufficient condition for producing time-dependent HFIs, the EC process being necessary to produce extra electronic holes. The absence of the dynamic interaction (in all ^{111m}Cd experiments in binary oxides) should be attributed to the time characteristics [$\tau_{1/2}(\gamma_1)$ very large] of the TDPAC probe rather than the absence of the electronic holes that the Auger process would produce after an EC decay if present. A similar result was observed in TDPAC studies in insulators using ^{199m}Hg and ^{204m}Pb as probes [59], with $\tau_{1/2}(\gamma_1) = 42.7$ and 66.9 min, respectively.

The last kind of nuclear decay that precedes a TDPAC probe is β^-. Among them, the second most employed TDPAC

probe is ^{181}Hf $(\beta^-) \rightarrow {}^{181}$Ta, for which there is absolutely no evidence in dynamic HFI of this type in insulators. Here, Ta^{5+} is a donor impurity in the oxides investigated by TDPAC in general, but the underlying cause for the absence of AE must be the extraordinarily long half-life of $\tau_{1/2}(\gamma_1) = 17.8\,\mu$s in comparison with the average recovery time of the electronic defect (electronic hole or donor electron). A particularly attractive probe to test our hypothesis further is ^{111}Ag $(\beta^-) \rightarrow {}^{111}$Cd since $\tau_{1/2}(\gamma_1) = 27$ ps is a very short time to observe the electronic relaxations, and the EFG would be measured also at a ^{111}Cd site, allowing a direct comparison with a large group of published observations. In theory, shake-off events originating in the β^- decay may result in electronic relaxation as the Auger process; however, the possibility of this occurrence is extremely low, and most ions will lose only one electron, implying that any dumping will be very weak. Rita *et al.* [61] conducted one experiment with ^{111}Ag $[(\beta^-) \rightarrow {}^{111}$Cd]-implanted ZnO that supported the low incidence of the shake-off process; however, it was only carried out at RT. Because the isovalent Cd does not produce electronic holes in this host, no obvious dynamic HFI was found.

Finally, we can mention that the β^+ decay compete with the EC route and could produce a similar scenario to that described for β^-, but no TDPAC experiments are reported in which this decay dominates over the EC.

Considering all this, we believe that, in the absence of EC decay of the probe nucleus, any acceptor or donor state introduced by the probe impurity in a semiconductor and whose ionization changes the EFG sensed by it will exhibit a time-dependent HFI, provided the lifetime of the nuclear levels that feed the γ_1 level of the γ_1-γ_2 cascade and this level itself is shorter than the lifetime of the recovery process (i.e., the lifetime of the electronic holes or the ionized donor electrons).

V. SUMMARY AND CONCLUSIONS

TDPAC measurements in high-purity polycrystalline SnO doped with $(^{111}\text{In} \rightarrow) {}^{111}$Cd as a probe atom were performed as a function of temperature in the range 20–900 K in a reversible way.

XRD characterization confirms the presence of only the SnO crystalline phase, not showing the development of other tin oxide phases when the sample is exposed to high temperatures in vacuum.

The TDPAC spectra showed a strong and characteristic damping in the first nanoseconds, which decreases (in a reversible way) as the measurement temperature increases, allowing us to analyze it using a time-dependent perturbation factor in the framework of the B-O on-off model.

Two HFIs, HFI1 (time dependent) and HFI2 (static), were necessary to account for the $R(t)$ spectra throughout the whole temperature range of measurements. The majority interaction HFI1, as specified by EFG1, is well defined and characterized by hyperfine parameters that are temperature independent, whereas the minority interaction HFI2, as defined by EFG2, has a subtle steplike behavior for V_{33} at ∼600 K. In the case of the time-dependent HFI1, the relaxation constant λ_r, which accounts for the attenuation strength caused by fluctuating EFGs producing a dynamic interaction, increases as T lowers. However, while $\tau_g = 1/\lambda_g$ (the lifetime of the electronic holes) diminishes as T increases, this interaction does not have a temperature threshold at which it becomes totally static, like the two HFI present in $(^{111}\text{In} \rightarrow) {}^{111}$Cd-doped SnO_2 [7]. Here, EFG1 and EFG2 are associated with any final stable electronic configuration of the ^{111}Cd probe once the dynamic regime is turned off in the B-O on-off model. In this sense, HFI2 is static since electronic recombination (i.e., the fluctuating regime) ceases before the time window of the TDPAC experiment begins.

The detailed *ab initio* calculations of the electronic structure of Cd-doped SnO revealed that the substitution of a Sn atom by a Cd impurity introduces a low number of delocalized Cd d and p states, resulting in an almost flat negligible distribution of electronic states at the TVB and the formation of an impurity empty level at the BCB, which is also a mixture of d and p states. Furthermore, the Cd impurity causes isotropic outward relaxations of the O_{NN} atoms. The p contribution governs the strong V_{33} variation as a function of the charge state of the SC at the Cd site, while the d contribution is practically independent of this charge state.

We can definitively assign HFI1 to ^{111}Cd probes localized at substitutional Sn sites free of defects (with the VB completely filled) and HFI2 to ^{111}Cd probes localized at substitutional Sn sites with an electronic hole trapped ($q = 1+$) by comparing the experimental results and the *ab initio* predictions of the EFG tensor, together with the formation energy calculation results.

Finally, based on the current *ab initio* work, which shows that the VB in Cd-doped SnO is entirely filled, we may infer that an acceptor level provided by the probe atom in a semiconductor or insulator is not required to observe the ECAE phenomena.

The information obtained here on the static HFI2 in SnO : ^{111}In provides us with a perspective on the origin of the dynamic ECAE phenomenon and a quantification of the number of holes responsible of the dynamic regime in SnO. Before the emission of γ_1, a minority fraction of probes (sensed by HFI2) reaches a stable electronic configuration, filling (all the probes) all the electronic holes of the EC (i.e., ∼7) except the outermost one. On the other hand, most probes (as identified by HFI1) fill this last hole after the emission of γ_1, resulting in the dynamic interaction, with the latter effect dependent on temperature and the electron availability of the host. This crucial information allowed us to calculate the number of electronic holes (only one in SnO : ^{111}In) involved in the generation of the dynamic effect, assuming that the off of the fluctuation of charge states occurs after the emission of γ_1. In this regard, the emission of γ_1 must be fast enough in comparison with the recovery time of the electronic hole.

In summary, we find that, in general, the occurrence of the EC decay is not necessary nor sufficient to induce this type of time-dependent interaction but that the $^{111}\text{In} \rightarrow {}^{111}$Cd isotope is capable of producing this effect on its own (the EC is sufficient in the case of this probe). We show that the acceptor character of the probe is not required if an appropriate probe $[\tau_{1/2}(\gamma_1) > 1\,\text{ns}]$ obtained through EC decay of its parent is employed.

Finally, we propose that, in the absence of EC decay of the probe nucleus of the parent, any probe impurity introducing

acceptor or donor states in a semiconductor or insulator and whose ionization changes the EFG sensed by it will observe a time-dependent HFI if the lifetime of the nuclear levels that feed the γ_1 level of the γ_1-γ_2 cascade as well as this level itself is shorter than the lifetime of the recovery process (i.e., the lifetime of the electronic holes or the ionized donor electrons). To conclusively test this hypothesis, TDPAC experiments as a function of temperature should be designed using an appropriate probe generated by β^- functioning as an acceptor in a binary oxide (e.g.,^{111}Ag doping SnO_2). Future studies in this area are envisaged.

ACKNOWLEDGMENTS

This paper was partially supported by CONICET under Grant No. PIP0803, Conselho Nacional de Desenvolvimento Científico e Tecnológico (CNPq) Grants No. 305046/2013-6 and No. 311373/2018-6, and Fundação de Amparo a Pesquisa do Estado de São Paulo (FAPESP) Grant No. 2014/14001-1. In this paper, we made use of the computational facilities of the Physics of Impurities in Condensed Matter group at IFLP and Departamento de Física (UNLP). Professor Dr. A. F. Pasquevich is gratefully acknowledged for very fruitful discussions about the time-dependent perturbation factor and the ECAE phenomena. Enlightening discussions about defect formation energy calculations by Prof. Dra. L.V.C. Assali are also kindly acknowledged. E.L.M. wishes to thank the personnel at IPEN for their kind hospitality during his research stay. H.M.P. acknowledges financial support from CNPq and FAPESP. G.N.D., D.R., and M.R. are members of CONICET, Argentina.

[1] T. Dietl, H. Ohno, F. Matsukura, J. Cibert, and D. Ferrand, Science **287**, 1019 (2000).
[2] Y. Matsumoto, M. Murakami, T. Shono, T. Hasegawa, T. Fukumura, M. Kawasaki, P. Ahmet, T. Chikyow, S. Koshihara, and H. Koinuma, Science **291**, 854 (2001).
[3] J. M. D. Coey, M. Venkatesan, and C. B. Fitzgerald, Nat. Mater. **4**, 173 (2005).
[4] J. Zhi, M. Zhou, Z. Zhang, O. Reiser, and F. Huang, Nat. Commun. **12**, 445 (2021).
[5] P. Kessler, K. Lorenz, and R. Vianden, Defect Diffus. Forum **311**, 167 (2011).
[6] A. F. Pasquevich and M. Rentería, Defect Diffus. Forum **311**, 62 (2011).
[7] G. N. Darriba, E. L. Muñoz, A. W. Carbonari, and M. Rentería, J. Phys. Chem. C **122**, 17423 (2018).
[8] A. G. Bibiloni, J. Desimoni, C. P. Massolo, L. Mendoza-Zélis, A. F. Pasquevich, F. H. Sánchez, and A. López-García, Phys. Rev. B **29**, 1109 (1984).
[9] A. G. Bibiloni, C. P. Massolo, J. Desimoni, L. A. Mendoza-Zélis, F. H. Sánchez, A. F. Pasquevich, L. Damonte, and A. R. López-García, Phys. Rev. B **32**, 2393 (1985).
[10] C. P. Massolo, J. Desimoni, A. G. Bibiloni, L. A. Mendoza-Zélis, L. C. Damonte, A. R. Lopez-Garcia, P. W. Martin, S. R. Dong, and J. G. Hooley, Phys. Rev. B **34**, 8857 (1986).
[11] W. Bolse, M. Uhrmacher, and J. Kesten, Hyperfine Interact. **35**, 931 (1987).
[12] K. Asai, F. Ambe, S. Ambe, T. Okada, and H. Sekizawa, Phys. Rev. B **41**, 6124 (1990).
[13] A. Bartos, K. P. Lieb, A. F. Pasquevich, and M. Uhrmacher, Phys. Lett. A **157**, 513 (1991).
[14] D. Lupascu, S. Habenicht, K.-P. Lieb, M. Neubauer, M. Uhrmacher, and T. Wenzel, Phys. Rev. B **54**, 871 (1996).
[15] S. Habenicht, D. Lupascu, M. Uhrmacher, L. Ziegeler, and K.-P. Lieb, Z. Phys. B **101**, 187 (1996).
[16] S. Habenicht, D. Lupascu, M. Neubauer, M. Uhrmacher, K. P. Lieb, and the ISOLDE-Collaboration, Hyperfine Interact. **120**, 445 (1999).
[17] J. Penner and R. Vianden, Hyperfine Interact. **158**, 389 (2004).
[18] U. Bäverstam, R. Othaz, N. de Sousa, and B. Ringström, Nucl. Phys. A **186**, 500 (1972).
[19] L. A. Errico, G. Fabricius, M. Rentería, P. de la Presa, and M. Forker, Phys. Rev. Lett. **89**, 055503 (2002).
[20] L. A. Errico, G. Fabricius, and M. Rentería, Phys. Rev. B **67**, 144104 (2003).
[21] E. L. Muñoz, D. Richard, A. W. Carbonari, L. A. Errico, and M. Rentería, Hyperfine Interact. **197**, 199 (2010).
[22] G. N. Darriba, M. Rentería, H. M. Petrilli, and L. V. C. Assali, Phys. Rev. B **86**, 075203 (2012).
[23] D. Richard, E. L. Muñoz, M. Rentería, L. A. Errico, A. Svane, and N. E. Christensen, Phys. Rev. B **88**, 165206 (2013).
[24] G. N. Darriba, L. A. Errico, P. D. Eversheim, G. Fabricius, and M. Rentería, Phys. Rev. B **79**, 115213 (2009).
[25] G. N. Darriba, E. L. Muñoz, L. A. Errico, and M. Rentería, J. Phys. Chem. C **118**, 19929 (2014).
[26] D. Richard, G. N. Darriba, E. L. Muñoz, L. A. Errico, and M. Rentería, J. Alloys Compd. **594**, 189 (2014).
[27] D. Richard, G. N. Darriba, E. L. Muñoz, L. A. Errico, P. D. Eversheim, and M. Rentería, J. Phys. Chem. C **120**, 5640 (2016).
[28] D. Richard, M. Rentería, and A. W. Carbonari, Semicond. Sci. Technol. **32**, 085010 (2017).
[29] M. Rentería, A. G. Bibiloni, M. S. Moreno, J. Desimoni, R. C. Mercader, A. Bartos, M. Uhrmacher, and K. P. Lieb, J. Phys. Condens. Matter **3**, 3625 (1991).
[30] L. A. Errico, M. Rentería, and H. M. Petrilli, Phys. Rev. B **75**, 155209 (2007).
[31] E. L. Muñoz, A. W. Carbonari, L. A. Errico, A. G. Bibiloni, H. M. Petrilli, and M. Rentería, Hyperfine Interact. **178**, 37 (2008).
[32] H. Frauenfelder and R. M. Steffen, *Alpha-, Beta-, and Gamma-Ray Spectroscopy*, edited by K. Seigbahn (North-Holland Publishing Co., Amsterdam, 1968).
[33] E. N. Kaufmann and R. J. Vianden, Rev. Mod. Phys. **51**, 161 (1979).
[34] G. Schatz and A. Weidinger, *Nuclear Condensed Matter Physics: Nuclear Methods and Applications* (Wiley, Chichester, 1996).
[35] M. Rentería, F. G. Requejo, A. G. Bibiloni, A. F. Pasquevich, J. Shitu, and K. Freitag, Phys. Rev. B **55**, 14200 (1997).
[36] A. Abragam and R. V. Pound, Phys. Rev. **92**, 943 (1953).

[37] L. A. Mendoza-Zélis, A. G. Bibiloni, M. C. Caracoche, A. R. Lopéz-García, J. A. Martínez, R. C. Mercader, and A. F. Pasquevich, Hyperfine Interact. **3**, 315 (1977).
[38] P. Herzog, K. Freitag, M. Reuschenbach, and H. Walitzki, Z. Physik A **294**, 13 (1980).
[39] J. Haines and J. M. Léger, Phys. Rev. B **55**, 11144 (1997).
[40] F. Lawson, Nature (London) **215**, 955 (1967).
[41] C. Decroly and M. Ghodsi, Comptes Rendus Acad. Sci. Série C: Sci. Chim. **261**, 2659 (1965).
[42] H. E. Swanson and E. Tatge, J. Res. Natl. Bur. Stand. **539**, 24 (1953).
[43] J. Pannetier and G. Denes, Acta Crystallogr. B **36**, 2763 (1980).
[44] F. Izumi, J. Solid State Chem. **38**, 381 (1981).
[45] P. Hohenberg and W. Kohn, Phys. Rev. **136**, B864 (1964).
[46] W. Kohn and L. J. Sham, Phys. Rev. **140**, A1133 (1965).
[47] G. K. H. Madsen, P. Blaha, K. Schwarz, E. Sjöstedt, and L. Nordström, Phys. Rev. B **64**, 195134 (2001).
[48] P. Blaha, K. Schwarz, G. Madsen, D. Kvasnicka, and J. Luitz, *WIEN2K, an Augmented Plane Wave Plus Local Orbitals Program for Calculating Crystal Properties* (Technical Universität, Wien, 2014).
[49] P. E. Blöchl, Phys. Rev. B **50**, 17953 (1994).
[50] K. Schwarz, C. Ambrosch-Draxl, and P. Blaha, Phys. Rev. B **42**, 2051 (1990).
[51] P. Blaha, K. Schwarz, and P. H. Dederichs, Phys. Rev. B **37**, 2792 (1988).
[52] M. Lederer and V. S. Shirley, *Table of Isotopes*, 7th Edition (John Wiley and Sons, New Jersey, 1978).
[53] M. Salomon, Nucl. Phys. **54**, 171 (1964).
[54] J. Zhang, Y. Han, C. Liu, W. Ren, Y. Li, Q. Wang, N. Su, Y. Li, B. Ma, Y. Ma, and C. Gao, J. Phys. Chem. C **115**, 20710 (2011).
[55] N. W. Ashcroft and N. D. Mermin, *Solid State Physics* (Brooks/Cole, Belmont, 1973).
[56] J. M. Adams and G. L. Catchen, Phys. Rev. B **50**, 1264 (1994).
[57] T. Wenzel, A. Bartos, K. P. Lieb, M. Uhrmacher, and D. Wiarda, Ann. Phys. **504**, 155 (1992).
[58] D. Richard, M. Rentería, A. W. Carbonari, M. Romero, and R. Faccio, Ceram. Int. **46**, 16088 (2020).
[59] H. Haas and D. A. Shirley, J. Chem. Phys. **58**, 3339 (1973).
[60] T. Butz and R. Vianden, Hyperfine Interact. **221**, 99 (2013).
[61] E. Rita, J. G. Correia, U. Wahl, E. Alves, A. M. L. Lopes, J. C. Soares, and The ISOLDE Collaboration, Hyperfine Interact. **158**, 395 (2004).